frontiers in Materials

ORIGINAL RESEARCH
published: 16 November 2020
doi: 10.3389/fmats.2020.597528

Bioethanol Steam Reforming over Cobalt-Containing USY and ZSM-5 Commercial Zeolite Catalysts

Gabriela Grzybek[1], Magdalena Greluk[2], Karolina Tarach[1], Kamila Pyra[1], Grzegorz Słowik[2], Marek Rotko[2] and Kinga Góra-Marek[1]*

[1]Faculty of Chemistry, Jagiellonian University, Krakow, Poland, [2]Faculty of Chemistry, University of Maria Curie-Sklodowska, Lublin, Poland

The ethanol steam reforming (ESR) process over cobalt-based zeolitic catalysts, differing significantly in the structure, was comprehensively examined. The cobalt spinel phase (10 wt%) was deposited on the surface of USY and ZSM-5 zeolites (Si/Al ratio of 31). The catalysts were characterized in terms of their chemical (ICP) and phase composition (XRD), textural properties (low-temperature N_2 adsorption), morphology (STEM/EDX), and reducibility (H_2-TPR). The aforementioned characteristics were supplemented by the catalysts' acidity and redox properties investigations (quantitative FT-IR studies of pyridine and carbon monoxide adsorption). Catalysts' activity was evaluated in the ESR process at 500°C for various ethanol/water mixtures. Both catalysts exhibited 100% ethanol conversion, whereas their selectivity toward H_2, CO_2, and C_2H_4 strongly depended on the applied ethanol-to-water molar ratio. Comparable selectivities observed for the 1 : 4 ratio were improved for the 1 : 9 ratio for both catalysts, as expected. For the ratio of 1 : 12, the significant difference in the reaction paths (the ethanol dehydration for CoUSY and the ethanol steam reforming for CoZSM-5) was explained by the cobalt reoxidation process facilitated by water molecules for the CoUSY. The superior overall performance of the CoZSM-5 catalyst in the ESR process, in comparison to CoUSY, also results from its almost three times enhanced accessibility of the cobalt species, as confirmed by the quantitative FT-IR studies of CO sorption. The microscopic studies also indicated a better dispersion of the cobalt phase supported on the ZSM-5 support. Thus, the structure of ZSM-5 zeolite assures higher cobalt active phase dispersion being more beneficial for the ESR process.

Keywords: cobalt catalyst, zeolite Y, zeolite ZSM-5, ethanol steam reforming, catalyst acidity

OPEN ACCESS

Edited by:
Miriam Navlani-García, University of Alicante, Spain

Reviewed by:
Maria A. Goula, Western Macedonia University of Applied Science, Greece
Martin Charles Wilding, Sheffield Hallam University, United Kingdom

****Correspondence:***
Gabriela Grzybek
g.grzybek@uj.edu.pl

Specialty section:
This article was submitted to Ceramics and Glass, a section of the journal Frontiers in Materials

Received: *24 August 2020*
Accepted: *08 October 2020*
Published: *16 November 2020*

Citation:
Grzybek G, Greluk M, Tarach K, Pyra K, Słowik G, Rotko M and Góra-Marek K (2020) Bioethanol Steam Reforming over Cobalt-Containing USY and ZSM-5 Commercial Zeolite Catalysts. Front. Mater. 7:597528. doi: 10.3389/fmats.2020.597528

INTRODUCTION

Hydrogen-derived energy sources are a sustainable and environmentally friendly alternative to the utilization of fossil fuels, for which the availability of reserves is subject to high uncertainty. This, combined with the negative impact of their combustion on the environment, grows the global interest in the development of renewable energy sources intensively. Paying attention to hydrogen as a green energy carrier is a derivative of its possible application in internal combustion engines or fuel cells for efficient electricity generation (Bion et al., 2010; Sekine et al., 2014; Ogo et al., 2015; Zanchet et al., 2015; Ogo and Sekine, 2020). Hydrogen is expected to become the main energy source and

long-term replacement for natural gas shortly. Nevertheless, the current hydrogen production relies heavily on the steam reforming of natural gas, coal, or light hydrocarbons. Consequently, the extensive use of hydrogen as a renewable and clean (CO_2-neutral) energy source is still a challenge and remains intensive research (Maggio et al., 1998; Armor, 1999; Alberton et al., 2007; Contreras et al., 2014; Lang et al., 2015). In light of the above, the conversion of biomass to ethanol and its use in the steam reforming to produce hydrogen constitutes an important research path in recent years (Ni et al., 2007).

The ethanol steam reforming process (ESR), defined by **Eq. 1**, is an endothermic reaction occurring at the temperature range of 400–800°C (Chica, 2013).

$$C_2H_5OH + 3H_2O \rightarrow 6H_2 + 2CO_2 \quad (1)$$

The high efficiency of hydrogen production with $H_2O/C_2H_5OH = 6$ and at low operating temperatures is highly desired. This reaction is, however, accompanied by parallel side reactions as decomposition, dehydration, dehydrogenation, hydrogenolysis, methanation, water-gas shift reaction, Boudart reaction, and finally coke formation (Haryanto et al., 2005; Mattos and Noronha, 2005; Vaidya and Rodrigues, 2006). The aforementioned side processes are the source of undesirable by-products such as C_2H_4, CO, CH_4, CH_3CHO, and $(CH_3)_2CO$. Among them, the most undesired path is the ethanol conversion to ethylene as the latter is easily transformed into the carbonaceous deposit. The ethanol dehydration to ethylene is undergone in the presence of acid sites (Tarach et al., 2016; Gołąbek et al., 2018). Therefore, the relative share of individual side reactions strongly depends on the acid/redox characteristic of the catalyst, but also on the applied reaction variables (e.g., temperature, $EtOH/H_2O$ ratio, and contact time).

Among catalysts considered for the steam reforming of ethanol, the oxide-supported noble metals (Rh, Ru, Pt, Ir, and Au) showed superior activity and stability (Freni, 2001; Breen et al., 2002; Liguras et al., 2003; Deluga et al., 2004; Sheng et al., 2004; Wanat et al., 2004; Mattos and Noronha, 2005; Hsiao et al., 2007; Ogo and Sekine, 2020). High cost limits their industrial application, and interest shifts to catalysts based on nonnoble metals such as Cu, Ni, and Co, of which cobalt-based catalysts seem to be the most promising systems (Freni et al., 2003; Comas et al., 2004; Kaddouri and Mazzocchia, 2004; Llorca et al., 2004; Benito et al., 2005; Frusteri et al., 2006; Song et al., 2007; Torres et al., 2007; Zhang et al., 2007; Contreras et al., 2014; Hou et al., 2015; Chen et al., 2020). A major role in the course of the ESR process over the cobalt catalysts is played by the cobalt oxidation state. However, the role of various Co species is still under debate. The highest activity is usually associated with the presence of both metallic Co^0 and Co^{2+} sites (Mattos et al., 2012; Zanchet et al., 2015; Sohn et al., 2016; Passos et al., 2017; Sohn et al., 2017). The DFT calculations implied that the C-C bond scission is favored on the Co^0 sites, while the water activation and the acetate species formation preferably occur on the Co^{2+} sites (Li and Wang, 2018; Li et al., 2019). The acetate pathway is thus preferred over the catalysts containing both these sites (Co^0 and Co^{2+}). The rapid reaction between the acetate species and water to form CO_x and H_2, without the involvement of the CH_4 formation, is responsible for the high performance of the Co-based catalysts in the ESR process (Sekine et al., 2014; Ogo et al., 2015; Ogo and Sekine, 2020). In turn, Inokawa et al. (2010) reported the rapid C_2H_4 production by ethanol dehydration in the presence of transition Co^{2+} and Ni^{2+} cations in the zeolites Y.

The main drawback of using the nonnoble metal catalysts, including those based on cobalt, is their rapid deactivation under reaction conditions. Both sintering and coke formation can, however, be limited by selecting appropriate support. The influence of the oxide-support on the catalyst activity in the ESR process was documented for several materials such as Al_2O_3, SiO_2, ZrO_2, Nb_2O_5, MgO, and CeO_2 (Llorca et al., 2002; Frusteri et al., 2004; Benito et al., 2005; Frusteri et al., 2006; Contreras et al., 2014; Riani et al., 2020). The role of support is to enhance the dispersion of the metallic active phase by metal-support interaction leading to an improvement of catalytic performance as well as to a reduction of carbon species forming during the process. High surface area and the porous structure can both assure high dispersion of metallic species and increase their resistance against sintering (Llorca et al., 2002; Da Costa-Serra et al., 2010). Thus, the zeolites with a microporous system of channels and cages typically offering high thermal stability and surface area around 400–800 m^2g^{-1} seem to be attractive candidates for supporting the metal-originating species (Campos-Skrobot et al., 2008; Chica and Sayas, 2009; Da Costa-Serra and Chica, 2011; Inokawa et al., 2011; Calles et al., 2020; Wang et al., 2020).

The early report on Cu-zeolites used for the ESR process can be found in 2001 (Łaniecki, 2001), whereas those concerning the catalytic steam reforming of ethanol started to appear in the 1990s (García and Laborde, 1991; Haga et al., 1997; Trimm, 1999). The role of zeolites as supports was raised again in the work of Campos-Skrobot et al. (2008). The Rh catalyst supported on the NaY zeolite allowed achieving the 68% yield of H_2. Vizcaino et al. reported Cu–Ni-based catalyst supported on nanocrystalline ZSM-5 zeolites for the ESR; however, the optimal identified operating temperature was 600°C (Vizcaíno et al., 2007). Chica et al. (Chica and Sayas, 2009; Da Costa-Serra and Chica, 2011) have proposed the use of delaminated pure silica ITQ-2 and ITQ-18 zeolites as a highly active and stable catalyst for the ESR process. Nevertheless, the cost-effective materials are still in high demand for industrial applications.

Thus, the present paper focuses on the use of commercially available ZSM-5 and USY zeolites as supports for Co-catalysts. Both applied zeolites are used as catalysts in the most important conversion processes used in petroleum refineries (fluid catalytic cracking). Both offer the three-dimensional porous network with interconnected channels varying in size; slightly larger pores openings are found in the USY zeolite than in the ZSM-5 and high thermal stability. As the acidic function of zeolites is responsible for the undesirable dehydration of ethanol, leading to coke formation, the high Si/Al ratio zeolites were selected.

Since the ethanol-to-water ratio is a key factor in the ESR reaction, the catalysts were extensively tested at variable water content ($EtOH/H_2O$ equal to 1 : 4, 1 : 9, and 1 : 12). Although the reaction stoichiometry determines the ethanol-to-steam (EtOH/

H_2O) molar ratio of 1 : 3, the use of excess water is advisable because bioethanol produced renewable in the fermentation process of biomass is a mixture of ethanol and water with a molar ratio of 1 : 7 to 1 : 13. Hence, it is advantageous to use bioethanol directly, i.e., without an energy-consuming ethanol distillation process, as this allows the final fuel cost to be minimized (Ni et al., 2007; Subramani and Song, 2007; Llorca et al., 2013; Bineli et al., 2016; Ghasemzadeh et al., 2019). Moreover, the excess water favors the water-gas shift reaction which is particularly important because it converts CO to CO_2 and H_2 products (Subramani and Song, 2007; Bineli et al., 2016; Zhurka et al., 2018). Therefore, to maximize the amount of H_2 produced, it is essential to ensure a sufficient supply of water (Comas et al., 2004; Ni et al., 2007; Ghasemzadeh et al., 2019). Furthermore, it is also well known that carbon formation can be minimized by gasification with steam, which means that the excess of water allows for reducing the formation of carbon deposits (Comas et al., 2004; Bineli et al., 2016).

The co-modified zeolitic catalysts (CoUSY and CoZSM-5) were thoroughly characterized by means of XRD, TEM/EDX, TPR, and FT-IR sorption studies to define the effect of the co-moieties dispersion and metal-support interactions on their catalytic performance in the ESR process carried out at variable water content.

EXPERIMENTAL

Materials

The super dealuminated ultrastabilized zeolite H-SDUSY (Si/Al = 31, CBV 760, labeled USY) was purchased from the Zeolyst Company. In turn, the proton form of the zeolite ZSM-5 (Si/Al = 31) was obtained by converting the ammonium form (Zeolyst, CBV 5524G) by calcination at 500°C for 2 h with a rate of 2°C/min. The cobalt in the amount of 10 wt% was introduced onto the surface of both zeolites by incipient wetness impregnation method from aqueous solution of cobalt(II) nitrate(V) (Aldrich). The final materials were dried at RT and then calcined under the condition indicated above.

Catalysts Characterization

The Si/Al ratio in the studied zeolites was verified using a Perkin Elmer Optima 2100DV ICP-OES spectrometer. Powder X-ray diffraction spectra were obtained using a Rigaku Multiflex diffractometer using Cu Kα radiation (40 kV, 40 mA). The diffractograms were recorded in the 2θ angle range of 10–50° (step size of 0.02° and the accumulation time of 3 s).

The texture of the native and Co-loaded zeolites was analyzed by N_2-physisorption at −196°C using a Quantachrome Autosorb-1-MP gas sorption instrument. Before the measurement, the sample was outgassed under a high vacuum at 350°C for 16 h. The micropore volume was calculated using the t-plot method, while the Brunauer–Emmet–Teller method together with Rouquerol et al. (2007) recommendations was applied to calculate the apparent specific surface area. The pore volume values were derived from the Barrett–Joyner–Halenda model using the adsorption branch (Barrett et al., 1951).

The morphology and cobalt phase dispersion, as well as phase composition of the fresh catalysts, were studied using the electron microscope, Titan G2 60–300 kV (FEI Company) with an accelerating voltage of the electron beam equal to 300 kV (the details of sample preparation, apparatus, and the experimental procedure described elsewhere (Słowik et al., 2016; Grzybek et al., 2020)). The mapping was carried out in the STEM mode by collecting point by point EDS spectrum of each of the corresponding pixels in the map. The collected maps were presented in the form of a matrix of pixels with the color mapped significant element and the intensity corresponding to the percentage of each element. Phase separation in the cobalt-based catalysts was performed with the FFT by using masking available in the Gatan DigitalMicrograph software package.

The acidic properties of examined samples were assessed from quantitative FT-IR studies of pyridine (Py, ≥99.8%, Sigma-Aldrich) adsorption. Before the measurements, the catalysts in the form of pellets were evacuated *in situ* in a quartz IR cell at 500°C under the pressure of 10^{-6} mbar for 1 h. The first step of the pyridine adsorption quantitative procedure was the neutralization of all acid sites at 130°C with the Py vapor under static conditions. Afterward, the nonchemisorbed Py molecules share was removed by the evacuation at the same temperature and the spectrum was collected. The intensities of the Py bands at 1545 cm^{-1} (pyridinium ions, PyH^+) and at 1,450 cm^{-1} (Py coordinatively bonded to Lewis sites, PyL) were used to calculate the concentration of the acid sites. The following values of the absorption coefficients 0.07 $cm^2 \cdot \mu mol^{-1}$ for the 1545 cm^{-1} band of PyH^+ and 0.10 $cm^2 \cdot \mu mol^{-1}$ for the 1,450 cm^{-1} band of PyL were applied. In addition, the sorption of carbon monoxide (Linde Gas Poland, 99.95%), being a probe molecule differentiating the nature of the cobalt moieties, was performed. The sorption of the small doses of CO was carried out at −100°C up to the total saturation of all the electron acceptor acid sites, which was manifested by the maximum intensities of the bands in the 2,300–2,180 cm^{-1}. All the spectra presented in this work were recorded by gathering 300 scans with a resolution of 2 cm^{-1} on a Vertex 70 spectrometer (Bruker) equipped with an MCT detector.

The temperature-programmed reduction (H_2-TPR) of tested catalytic materials was carried out in the AutoChem II 2920 analyzer (Micromeritics, United States) with the linear temperature increase (10°C/min) from room temperature to 900°C. A reducing mixture (5 vol% of H_2 in Ar) was supplied into the quartz reactor (filled with 50 mg of a catalyst sample) at a rate of 30 cm^3/min. The consumption of hydrogen was measured by an early calibrated thermal conductivity detector after removing water with a freezing trap.

Catalysts Performance in the Ethanol Steam Reforming Reaction

The activity and selectivity of cobalt-containing zeolite catalysts in the ESR reaction were determined in a continuous fixed-bed quartz reactor (Microactivity Reference unit, PID Eng & Tech.) at 500°C. To avoid the hot spot, 100 mg of catalyst (0.15–0.3 mm) was diluted with quartz grains. The catalyst prior to the reaction

was reduced in hydrogen at 550°C for 1 h. The EtOH/H_2O mixture with a molar ratio of 1 : 12, 1 : 9, or 1 : 4 was fed from a pressurized container using a mass controller (Bronkhorst) to an evaporator maintained at 150°C. In order to obtain a constant ethanol concentration of around 7.7 mol% for each molar ratio, the reactant vapors were fed to the reactor at a flow rate of 100 ml min^{-1} without diluting with any inert gas for the molar ratio of 1 : 12, at a flow rate of 77 ml min^{-1} diluted with argon with the flow rate of 23 ml min^{-1} for the molar ratio of 1 : 9, and at a flow rate of 38.5 ml min^{-1} diluted with argon with the flow rate of 61.5 ml min^{-1} for the molar ratio of 1 : 4. The analysis of feed composition (all in the gas phase) was carried out online by means of two gas chromatographs (Bruker 450-GC and Bruker 430-GC). Details on the chromatography equipment have been previously reported elsewhere (Greluk et al., 2020a; Greluk et al., 2020b).

The conversion of ethanol (X_{EtOH}) and the selectivity to carbon-containing products (X_{CP}) were determined from

$$X_{EtOH} = \frac{C^{in}_{EtOH} - C^{out}_{EtOH}}{C^{in}_{EtOH}} \times 100\% \quad (2)$$

$$X_{CP} = \frac{n_i C^{out}_i}{\sum n_i C^{out}_i} \times 100\% \quad (3)$$

where C^{in}_{EtOH} is the molar concentration of ethanol in the reaction mixture (mol%); C^{out}_{EtOH} is the molar concentration of ethanol in the postreaction mixture (mol%); C^{out}_i is the molar concentration of carbon-containing product in the postreaction mixture (mol %); n_i is the number of carbon atoms in carbon-containing molecule of the reaction product.

The selectivity of hydrogen formation was calculated from

$$H_2 selectivity = \frac{C^{out}_{H_2}}{C^{out}_{H_2} + 2 \times C^{out}_{CH_4} + 2 \times C^{out}_{C_2H_4} + 2 \times C^{out}_{CH_3CHO} + 3 \times C^{out}_{(CH_3)_2CO}} \times 100\% \quad (4)$$

where C^{out} is the molar concentration of the hydrogen-containing products in the postreaction mixture (mol%).

RESULTS AND DISCUSSION

Physicochemical Characterization

The Si/Al ratio of the reference zeolite supports, CoUSY and CoZSM-5 cobalt catalysts, determined by ICP, was found to be equal to 31 for each sample. From the X-ray diffractograms collected in **Figure 1**, it can be inferred that there was almost no change in the crystal structure of USY zeolite or ZSM-5 zeolite after the cobalt addition. Both, positions and intensities of the diffraction lines representative of the FAU and MFI structure, respectively, remained practically unaffected. Moreover, the additional low-intensity lines (marked by *) at 2θ equal to 31.2 and 36.9 in the diffraction patterns of CoUSY and CoZSM-5 catalysts were identified as corresponding to the (220) and (311) reflection planes of Co_3O_4 (ICSD 69378), respectively. The minor share of the cobalt phase in the registered diffractograms indicates its effective distribution in the as-prepared materials.

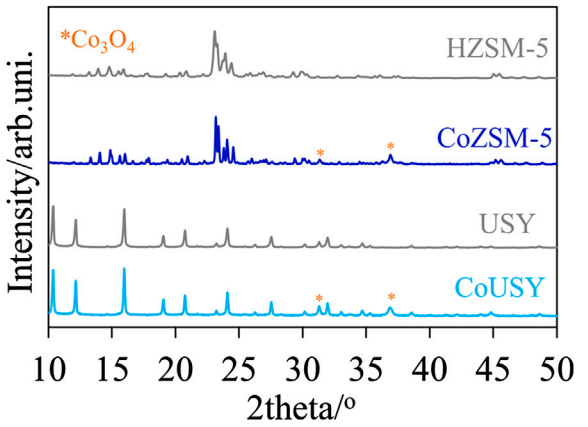

FIGURE 1 | XRD patterns of the CoUSY and CoZSM-5 catalysts as well as reference zeolite supports.

The chemical and structural characterization of the studied materials was complemented by the textural and morphological analysis. In general, the textural properties of both zeolite supports after impregnation with cobalt have been maintained (**Table 1**). Surprisingly, their microporosity did not decrease, indicating that the entire spinel cobalt phase covered the outside of the zeolite support grains and did not plug the micropores of the zeolites. On the other hand, the detected growth in the mesopore surface area (S_{meso}) (for the CoUSY catalyst) and mesopore volumes (V_{meso}) (for the CoUSY and CoZSM-5 catalysts) indicates a slight contribution of the cobalt spinel nanocrystals, located on the external surface of the zeolite grains, to the development of the catalyst mesoporosity.

The mentioned external location of the spinel cobalt phase was confirmed by the microscopic observations (**Figure 2**). HRTEM images of both CoUSY and CoZSM-5 samples (**Figures 2A$_1$–A$_2$,B$_1$–B$_2$**) show supports' particles with various shapes (mainly like a rectangle or coffin-shaped for the ZSM-5). On the external surface of the zeolite crystals, the cobalt species (dark places) are dispersed (**Figures 2A$_3$,B$_3$** and **3A,B$_1$**). Yet, the dispersion of the cobalt phase differs significantly for studied catalysts. The cobalt phase is forming on the USY zeolite surface large flattened agglomerates (**Figure 2A$_2$**), while in the case of the CoZSM-5 sample, a significant amount of small cobalt phase crystallites is present (**Figure 2B$_2$**). Phase identification of the CoUSY and CoZSM-5 catalysts, which was obtained based on the HRTEM images (**Figures 3A$_1$,B$_1$**) and FFT (Fast Fourier

TABLE 1 | Textural properties (from low-temperature N_2 physisorption) of the studied cobalt catalysts and reference zeolites.

Sample	S_{BET}/ $m^2.g^{-1}$	S_{micro}/ $m^2.g^{-1}$	S_{meso}/ $m^2.g^{-1}$	V_{micro}/ $cm^3.g^{-1}$	V_{meso}/ $cm^3.g^{-1}$
HZSM-5	380	340	40	0.15	0.07
CoZSM-5	385	350	36	0.15	0.10
USY	765	670	95	0.33	0.20
CoUSY	813	725	202	0.30	0.28

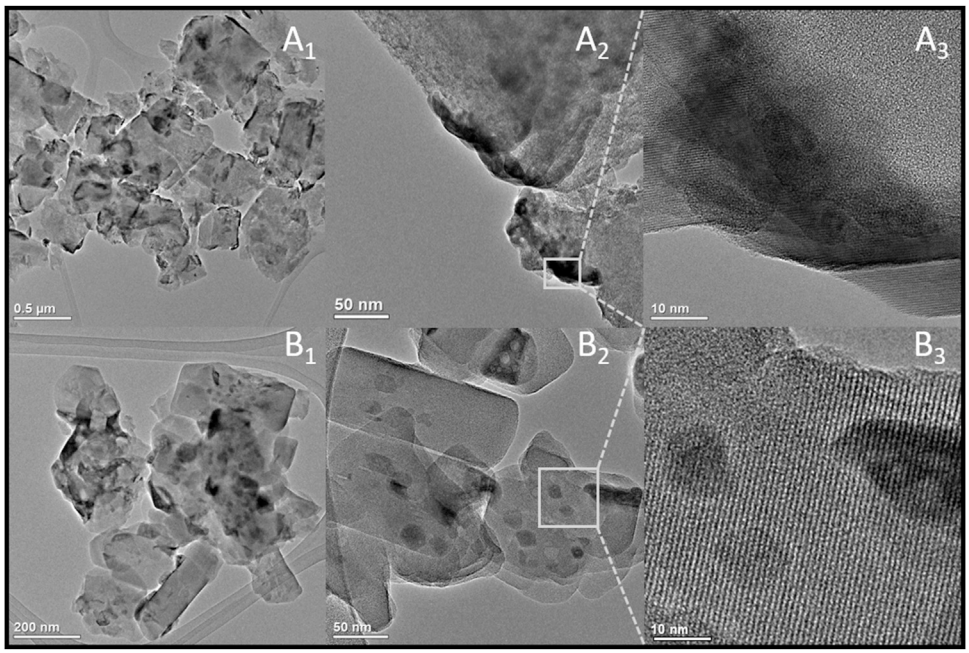

FIGURE 2 | HRTEM characteristics of the CoUSY **(A_1–A_5)** and CoZSM-5 **(B_1–B_5)** samples.

Transform) (**Figures 3A_2,B_2**), indicates that cobalt is present in the form of Co3O4 spinel in both samples. In the case of the CoUSY sample, it is confirmed by the following interplanar distances determined based on FFT: 2.44, 1.85, and 1.55 and corresponding to the lattice plane (311), (331), and (511), respectively, whereas the following interplanar distances and corresponding lattice planes were obtained for the CoZSM-5 catalyst: 2.85, 2.44 Å, and (220) and (311), respectively.

The local EDX analysis let us expose differences in the cobalt phase dispersion in the catalysts studied. As shown in **Figure 4**, the materials differ significantly in terms of the spinel crystallites' shape and size. In the case of CoUSY, the cobalt phase is mainly present in the form of flattened, long (100–200 nm) grains, while in the case of CoZSM-5, apart from such large crystallites, the small crystallites with sizes in the range of 10–100 nm are highly populated.

Acidic Properties (FT-IR Studies of Pyridine and CO Sorption)

The cobalt catalysts and reference zeolite supports were thoroughly characterized in respect to the nature, number, distribution, and strength of their acid sites by the FT-IR spectroscopy using pyridine and CO probe molecules. The results of pyridine sorption studies provided information on the total number of Brønsted (B) and Lewis (L) acid sites. In turn, the CO sorption studies enabled us to distinguish between Lewis acid sites of different origin and strength, which is documented by the various positions of the bands of CO interacting with them. For both used zeolite supports, the IR spectra of pyridine sorption (**Figure 5**) show the presence of the band at 1545 cm^{-1} and two bands at 1,445 and 1,455 cm^{-1}, corresponding to Py interacting with protonic and Lewis acid sites, respectively. The cobalt spinel deposition led to the generation of a significant number of Lewis acid sites of the strength different than found for protonic forms, giving an intense peak at 1,450 cm^{-1}. On the other hand, a noticeable decrease in the intensity of PyH^+ ions band upon cobalt deposition results from the replacement of the H^+ in exchangeable positions with the cobalt cations.

The concentration of the B and L acid sites in studied materials determined by pyridine is summarized in **Table 2**. The total acidity being the sum of Brønsted and Lewis sites corresponds well to the Al concentration determined from ICP analysis for the ZSM-5 zeolite. Still, it is significantly lower (about 24%) for the USY zeolite. Due to the framework geometry, the location of some H^+ in sodalite cages or hexagonal prisms make them inaccessible for pyridine molecule. Also, the copresence of nonacidic extraframework aluminum species cannot be excluded. Assuming that the impregnation procedure with the cobalt(II) salt solution did not affect the concentration of aluminum-originated Lewis sites, the enhancement in the amount of Lewis sites after Co-deposition was explicitly ascribed to cobalt(II) ions ($Co_{(Py)}$). In other words, the latter parameter was defined as the difference between the number of Lewis sites in the cobalt zeolite catalysts and corresponding proton zeolite forms (**Table 2**). The Py sorption studies revealed more than twice the concentration of Co-originated Lewis sites for the catalyst based on ZSM-5 zeolite support, demonstrating much better accessibility of the cobalt sites in this matrix. Worse accessibility of cobalt species in the CoUSY zeolite catalyst in combination with diffusion effects may affect

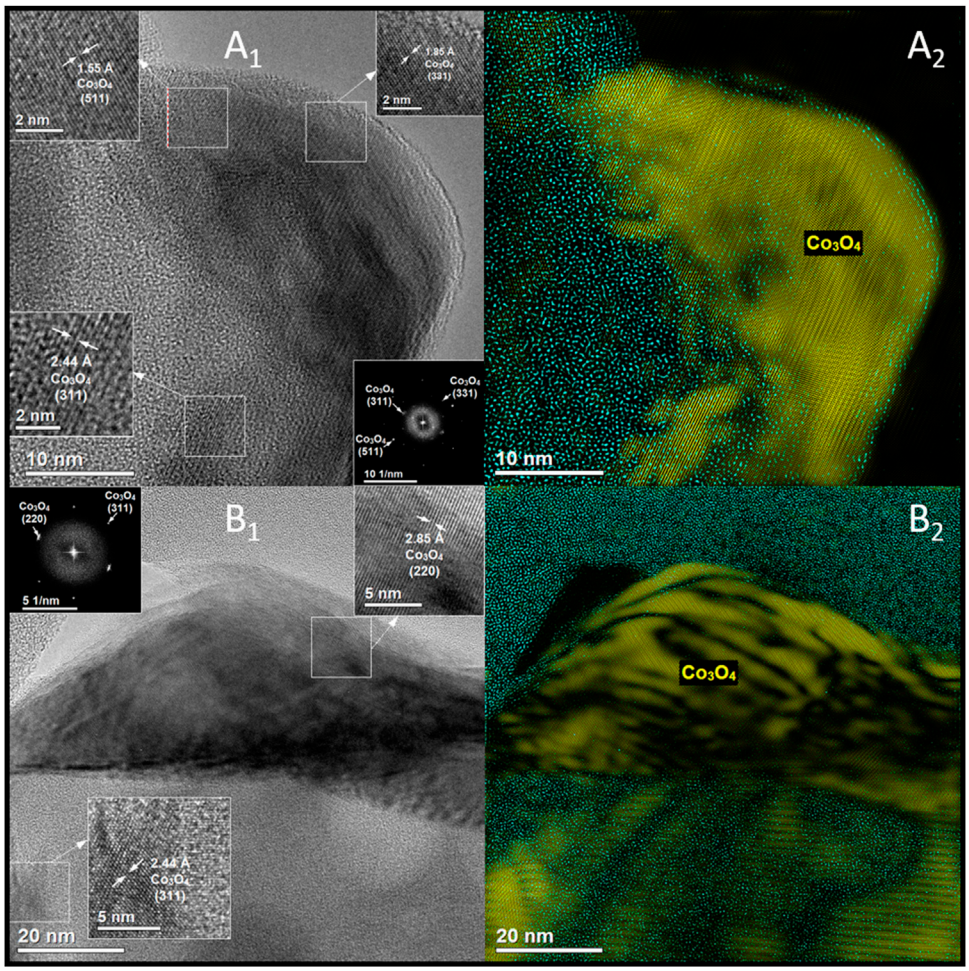

FIGURE 3 | HRTEM images together with FFT and phase identification of the CoUSY **(A_1,A_2)** and CoZSM-5 **(B_1,B_2)** samples.

the efficiency of the ESR reaction, providing premises for better performance of the CoZSM-5 catalyst.

The spectra of CO adsorbed on the zeolite supports (H-forms) and cobalt-containing catalysts are presented in **Figure 6**. The only band results from CO bonded to the Brønsted acid sites of H-zeolites is located at the frequency of 2,179 and 2,175 cm^{-1}, for USY and H-ZSM-5, respectively. No band in the frequency range of 2,300–2,180 cm^{-1} suggests no presence of Lewis electron acceptor sites. However, the presented above results of pyridine sorption studies indicate the presence of a small number of Lewis centers in H-zeolites (**Figure 5**). This discrepancy between the data obtained from CO and Py sorption can easily be explained by a significant difference in the basicity of probe molecules. The lower basicity of CO causes that the Lewis centers with low acidic strength will not be detectable by this probe (gas basicity of 898.1 for Py vs. 402.2 kJ/mol for CO) (Hunter and Lias, 1998).

In the case of cobalt-modified zeolites, the CO sorption studies indicated that the introduction of cobalt generates a significant number of Lewis sites. According to literature reports (Góra-Marek et al., 2007 and references therein), the appearance of bands in the range of 2,193–2,180 cm^{-1} is associated with the binding of the CO molecule by cobalt oxide centers. The higher CO band frequency observed in the CoUSY catalyst in comparison to CoZSM-5 is indicative of the stronger electron acceptor properties of the cobalt sites binding the CO molecule in the former. It is consistent with the TPR results presented further (**Figure 7**). In turn, the CO bands at 2,215 cm^{-1} (CoUSY) and 2,206 cm^{-1} (CoZSM-5) can be attributed to CO molecules coordinated to isolated cobalt(II) ions located in the exchangeable positions. As in the case of cobalt oxide-like centers, the higher frequency of Co^{2+} monocarbonyl band for the CoUSY catalyst points to stronger electron acceptor properties of its Co^{2+} ions.

Based on the methodology of quantitative measurement developed for cobalt sites in zeolites (Góra-Marek et al., 2009), the concentrations of isolated cobalt ions and cobalt ions in oxide forms were determined (**Table 2**). In general, there are similar trends for the CO and Py sorption studies: higher cobalt sites concentration was determined for the CoZSM-5 catalyst. However, the total number of cobalt sites from Py sorption studies is ca. twice of the one from CO

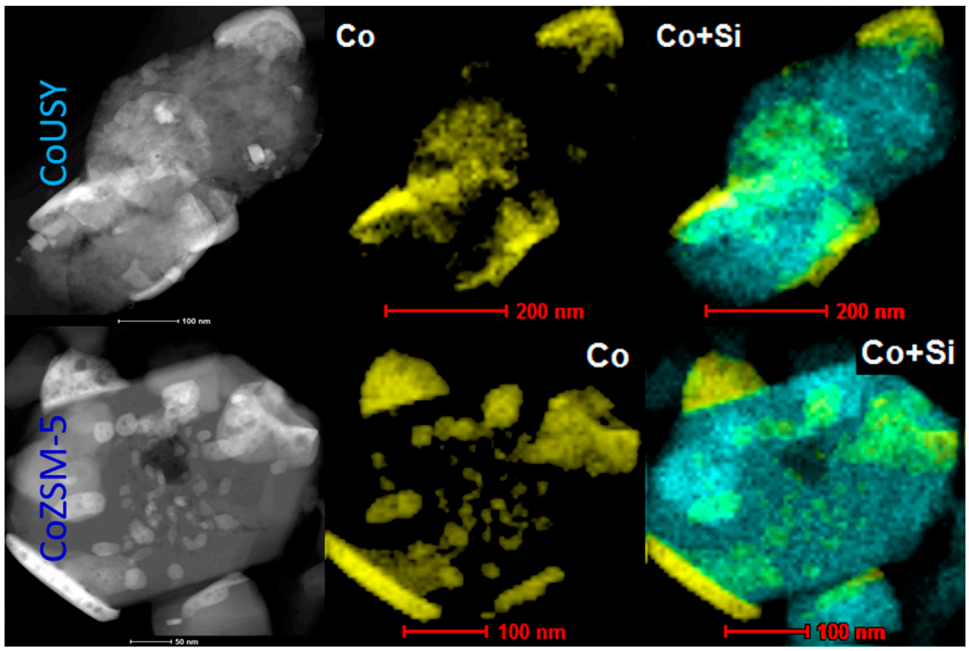

FIGURE 4 | HAADF/STEM images along with EDX maps of Co (yellow) and Si (blue) distributions in the CoUSY and CoZSM-5 catalysts.

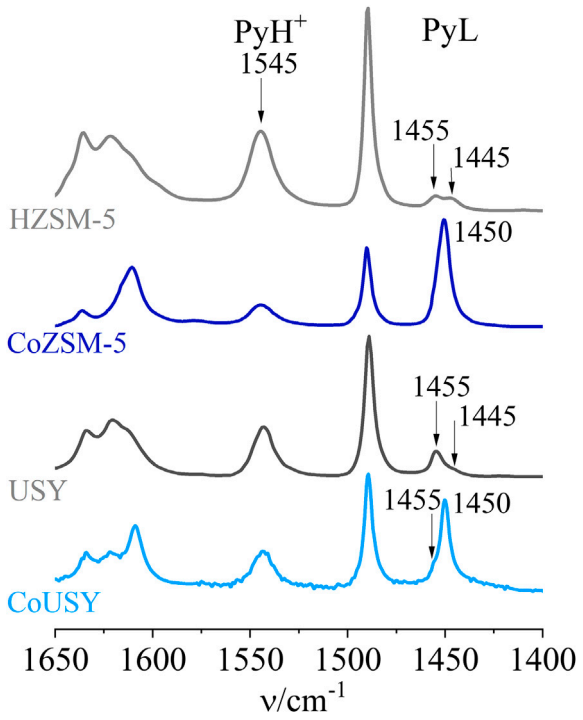

FIGURE 5 | IR spectra of pyridine sorption for the CoUSY and CoZSM-5 catalysts juxtaposed with the spectra of reference zeolite supports.

TABLE 2 | The content of Al, Brønsted (B), and Lewis (L) acid sites, in studied samples (Co-catalysts and reference zeolites) together with the content of Co species such as Co^{2+} ions and oxide-like cobalt forms (OLC) in the CoZSM-5 and Co-USY catalysts.

Sample	Al[a]	B[b]	L[b]	B + L[b]	Co-originated Lewis acid sites			
					$Co_{(Py)}$[b]	$Co^{2+}_{(CO)}$[c]	$OLC_{(CO)}$[c]	$(Co^{2+} + OLC)_{(CO)}$[c]
	μmol·g^{-1}				μmol·g^{-1}			
HZSM-5	472	445	70	515	—	—	—	—
CoZSM-5	472	247	328	575	258	62	77	139
USY	486	282	86	368	—	—	—	—
CoUSY	486	215	200	415	114	34	15	49

[a]*The concentration of Al from ICP analysis.*
[b]*The concentration of Brønsted (B) and Lewis (L) acid sites determined by FT-IR studies of pyridine adsorption.*
[c]*The concentration of Co^{2+} ions and oxide-like cobalt forms (OLC) determined by CO adsorption FT-IR studies (Góra-Marek et al., 2009).*

sorption studies. As mentioned above, it may be a consequence of a significant difference in the basicity of both probe molecules. The presented data revealed about two times higher total concentration of cobalt sites (Co^{2+} +OLC) capable of binding the pyridine molecule and almost three times higher total concentration of cobalt sites (Co^{2+} +OLC) capable of binding the CO molecule for the CoZSM-5 catalyst. Also, the greater preponderance of cobalt species concentration determined from CO sorption studies is probably a result of the limited accessibility of these species for a much bigger pyridine molecule. Thus, a fraction of Co sites in the CoZSM-5 catalyst detectable by CO may not be reached by the pyridine molecule. Assuming that only oxide-like cobalt forms are reduced to metallic Co^0, the CoZSM-5 catalyst provides nearly five times higher the number of

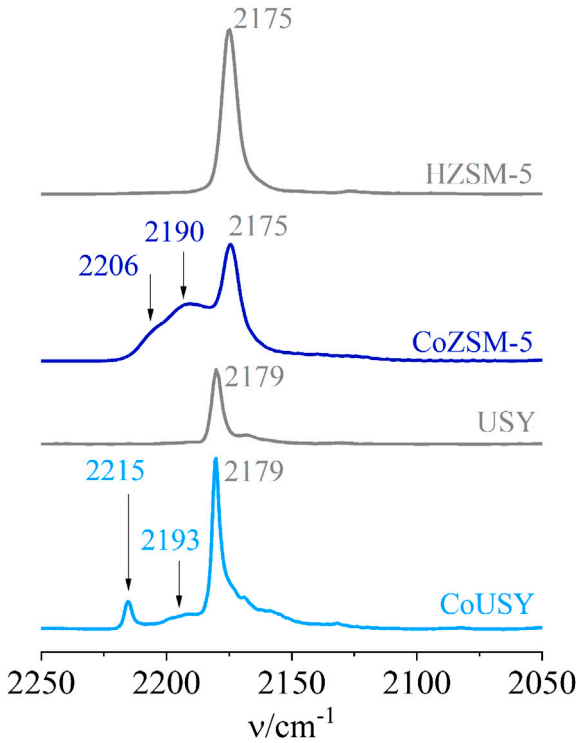

FIGURE 6 | IR spectra of CO sorption for the CoUSY and CoZSM-5 catalysts as well as reference zeolite supports.

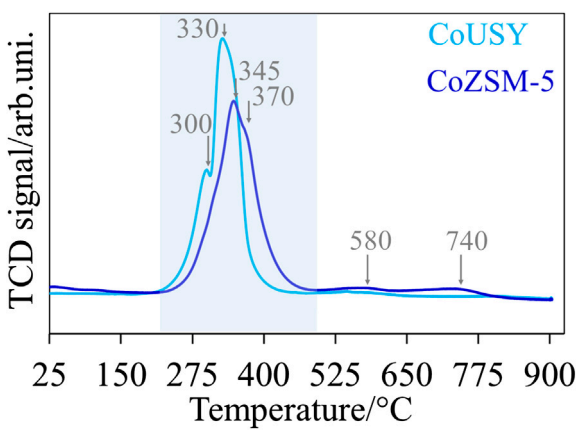

FIGURE 7 | H_2-TPR profiles of the CoUSY and CoZSM-5 catalysts.

metallic cobalt sites, i.e., the ESR process active sites, giving a premise to expect its better catalytic activity.

For both cobalt catalysts, the TPR profiles, collected in **Figure 7**, show two main reduction peaks in the temperature range of about 200–480°C, attributed to the reduction of cobalt oxide species (Grzybek et al., 2017) located on the external zeolite surface. These peaks centered at 300 and 330°C for the CoUSY catalyst are shifted toward the higher temperatures for CoZSM-5, to 345 and 370°C, respectively. This confirms the stronger electron acceptor properties of the CoUSY catalyst. Moreover, for the CoZSM-5 catalyst, additional low-intensity peaks at around 580 and 740°C can be noticed. Their presence is, most likely, related to the reduction of Co^{2+} in charge-compensating positions of the ZSM-5. It is further accompanied by a slight increase in the hydrogen consumption from 1.726 (for CoUSY) to 1.926 mmol H2/g (for CoZSM-5). The absence of these high-temperature peaks in the case of the CoUSY catalyst indicates the presence of a fraction of irreducible Co^{2+} ions, which does not participate in the ethanol steam reforming (Da Cruz et al., 1998; Wang et al., 2000). The presence of these irreducible ions is detected indirectly as the drop in the concentration of Brønsted acid sites after cobalt deposition (Py sorption IR studies).

The hydrogen consumption determined from the TPR profiles corresponds to approximately 76 and 85% of the total cobalt (10 wt%) contained in the CoUSY and CoZSM-5 catalysts, respectively, which indicates the presence of 24 and 15% of the irreducible cobalt species accordingly. On the other hand, the number of cobalt species determined by CO adsorption IR studies constitutes ca. 2.9 and 8.2% of that determined by H_2-TPR studies, indicating only partial accessibility of cobalt species. A significant share of cobalt, being enclosed inside the cobalt nanograins, is inaccessible for the CO probe molecule. Nevertheless, the amount of cobalt accessible in CoZSM-5 is almost 2.5 times higher than in CoUSY, which is consistent with the microscopic observations.

Catalysts Activity and Selectivity in the Ethanol Steam Reforming Process

The performance of the studied cobalt-containing in the ESR process carried out for ethanol-to-water molar ratio of 1 : 4, 1 : 9, and 1 : 12 is compared in **8** and **9**. The selectivity to the most important products, i.e., H_2, CO_2, and C_2H_4, is presented in **Figure 8**, while the residual products are presented in **Figure 9**. For both catalysts, the complete ethanol conversion (X_{EtOH} = 100%) is observed for 21 h of long time-on-stream tests for each studied ratio of 1 : 4, 1 : 9, and 1 : 12 (data not shown). The preliminary variability of the selectivity to reaction products over time results from the initial carbon deposition on the surface of the catalyst during side reactions. The selectivity of most of the products stabilized after about 6 h. After 21 h of the ESR reaction over the CoUSY catalyst, ca. 60%, 70%, and 30% of H_2 and ca. 25%, 35%, and 10% of CO_2 were produced at the EtOH/H_2O molar ratio of 1 : 4, 1 : 9, and 1 : 12, respectively (**Figure 10**). It means that the optimum the EtOH/H_2O molar ratio, which allows achieving the highest selectivity to two most desirable products of the ESR reaction, H_2, and CO_2, over the CoUSY catalyst is 1 : 9 (**Figure 10**). Surprisingly, the least amount of these products was formed not at the lowest water content (EtOH/H_2O molar ratio of 1 : 4) but the highest one (EtOH/H_2O molar ratio of 1 : 12). Regardless of the EtOH/H_2O molar ratio, CO selectivity was only ca. 5% after 21 h of the ESR reaction. It suggests that most of CO, occurring at the beginning of the process, was converted into CO_2 through the water-gas shift reaction (**Eq. 5**):

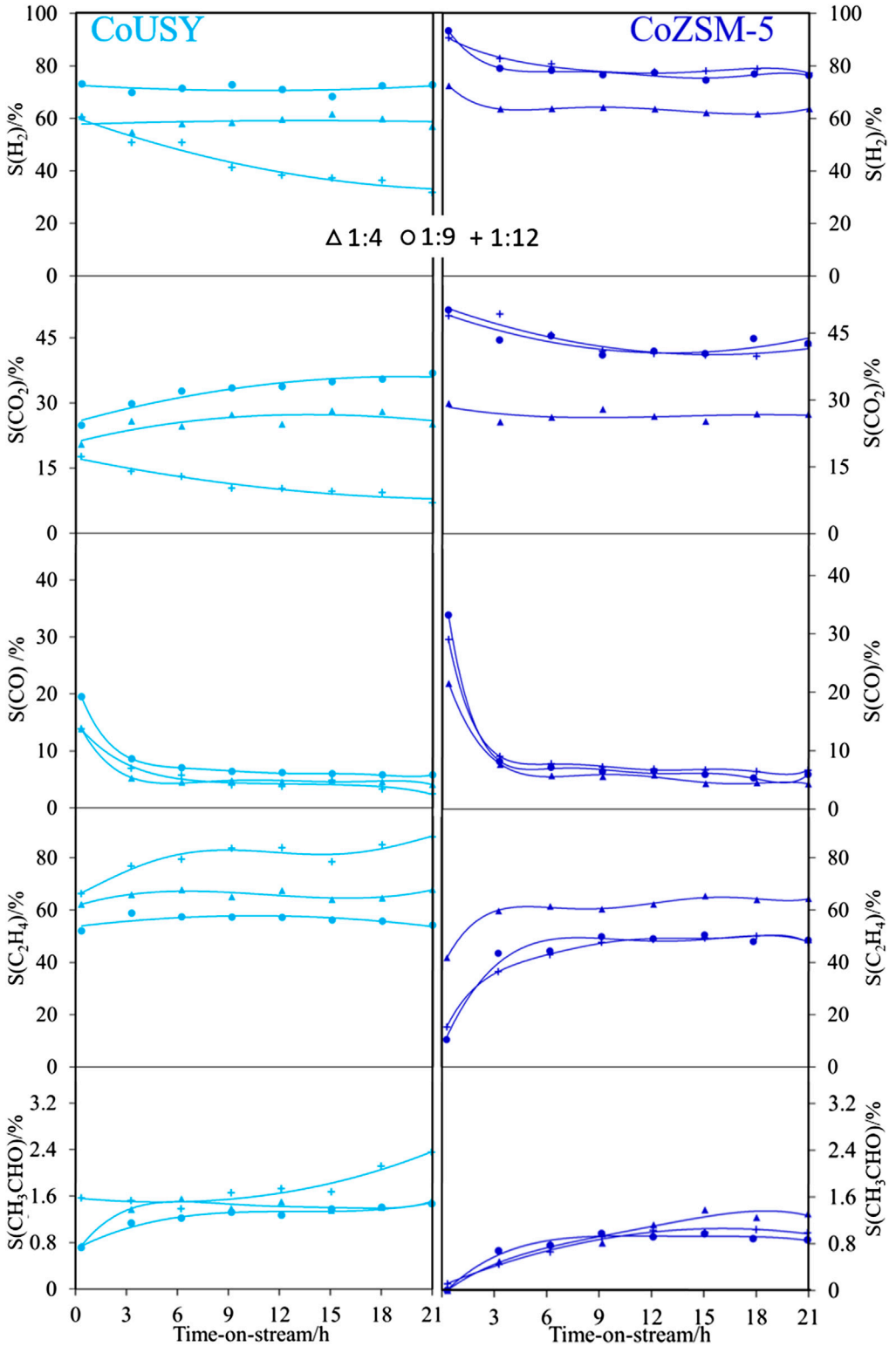

FIGURE 8 | Selectivity to the main products of the ESR process at 500°C for reaction mixtures with ethanol-to-water ratio of 1 : 4 (Δ), 1 : 9 (o), and 1 : 12 (+) for the CoUSY **(left column)** and CoZSM-5 **(right column)** catalysts.

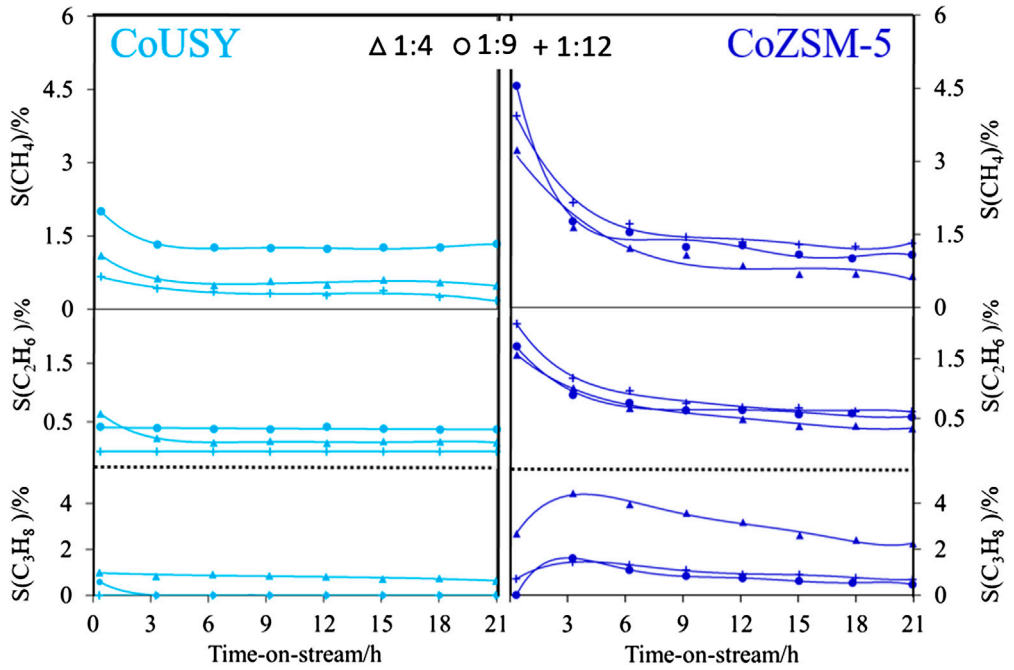

FIGURE 9 | Selectivity to residual products of the ESR process at 540°C for reaction mixtures with ethanol-to-water ratio of 1 : 4 (Δ), 1 : 9 (o), and 1 : 12 (+) for CoUSY **(left column)** and CoZSM-5 **(right column)** catalysts.

$$CO + H_2O \rightarrow CO_2 + H_2 \quad (5)$$

At the same time, the formation of C2 products (C_2H_4 and CH_3CHO) was the highest for the highest studied excess of water (EtOH/H_2O molar ratio of 1 : 12). Whereas the selectivity to CH_3CHO in the presence of the CoUSY catalyst is rather low at each studied EtOH/H_2O molar ratio (ca. 1.5% for 1 : 4 and 1 : 9 and ca. 2.5% for 1 : 12 after 21 h of the ESR), the number of C_2H_4 formed over this catalyst was significant (ca. 68%, 55%, and 88% for the EtOH/H_2O molar ratio of 1 : 4, 1 : 9, and 1 : 12, respectively). It indicates that ethanol dehydration to C_2H_4 (**Eq. 6**) was a dominant reaction while its dehydrogenation occurred to a lesser extent (**Eq. 7**):

$$C_2H_5OH \rightarrow C_2H_4 + H_2O \quad (6)$$

$$C_2H_5OH \rightarrow CH_3CHO + H_2 \quad (7)$$

Other hydrocarbons were produced over the CoUSY under the ESR conditions in much smaller quantities regardless of the EtOH/H_2O molar ratio (**Figure 9**). After 21 h of the ESR reaction, less than 1.5% of CH_4 and traces of C_2H_6 and C_3H_8 were detected. The formation of CH_4 can be ascribed to the direct decomposition of ethanol (**Eq. 8**) or acetaldehyde (**Eq. 9**), while C_2H_6 and C_3H_8 products probably resulted from the consecutive reactions of C_2H_4.

$$C_2H_5OH \rightarrow CH_4 + CO + H_2 \quad (8)$$

$$CH_3CHO \rightarrow CH_4 + CO \quad (9)$$

In the case of the CoZSM-5 catalyst, the increase of water content in the reaction mixture caused the enhancement of the process selectivity. After 21 h of the ESR reaction, selectivity to both H_2 and CO_2 increased from 64 to 77% and from 27 to 43%, respectively, with the change in EtOH/H_2O molar ratio from 1 : 4 to both 1 : 9 and 1 : 12 (**8** and **10**). After 21 h, also a similar amount of C_2H_4 (ca. 48%) was produced over the CoZSM-5 at both EtOH/H_2O molar ratios of 1 : 9 and 1 : 12, whereas selectivity to this product in the ESR reaction carried out at much lower water content (EtOH/H_2O molar ratio of 1 : 4) was much higher and equaled to ca. 64%. Similarly to results obtained for the CoUSY catalyst, the EtOH/H_2O molar ratio did not influence CO selectivity (ca. 6% for all EtOH/H_2O molar ratio after 21 h of ESR reaction). Other products, CH_3CHO (**Figure 8**), and hydrocarbons, CH_4, C_2H_6, and C_3H_8 (**Figure 9**), were detected in the presence of the CoZSM-5 catalyst in small quantities or even at trace level. Therefore, for both catalysts, the optimum EtOH/H_2O molar ratio, which allows achieving the highest selectivity to two main products of ESR reaction, was found to be 1:9. Still, more H_2 and CO_2 and fewer C_2H_4 were produced over the CoZSM-5 catalyst due to the better dispersion of the cobalt species. In turn, the influence of water (EtOH/H_2O equal to 1 : 12) observed for investigated catalysts was attributed to the water impact on the oxidation state of cobalt species. As reported by Varga et al. (2015) for the cobalt/ceria and rhodium-cobalt/ceria catalysts, the excess water can reoxidize the cobalt under reforming conditions. The authors reported that reoxidation occurs through the formation of water-induced Co oxides under the reforming condition. And since the Co^0/Co^{2+} ratio plays an important role in the catalyst activity in the ESR process (Ávila-Neto et al., 2013; Passos et al., 2014), the reoxidation appears to be of great importance. Thus, when the molar ratio of EtOH/H_2O is 1 : 12, the Co clusters may be

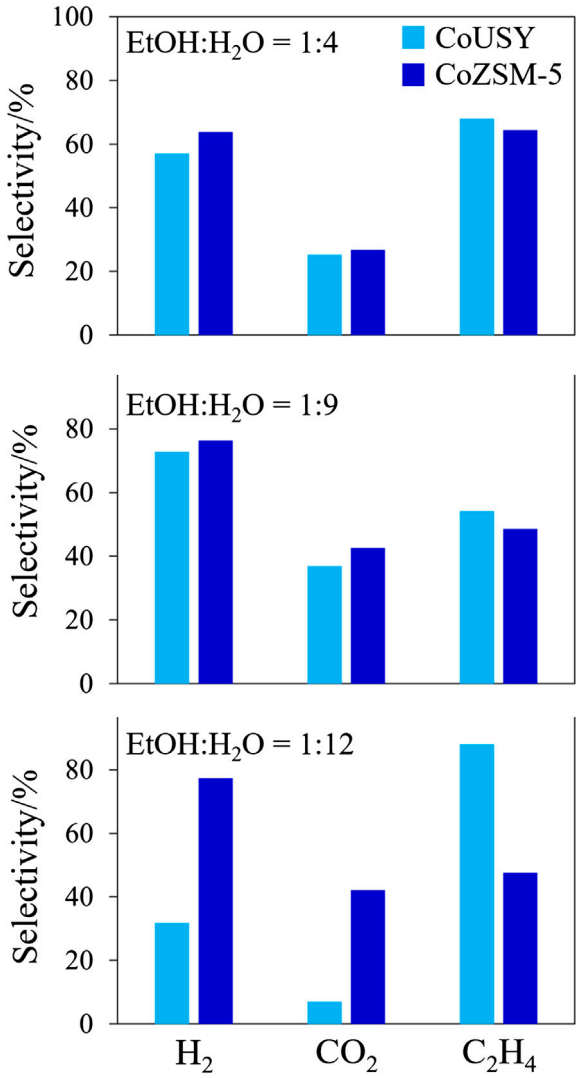

FIGURE 10 | The comparison of the selectivity to H_2, CO_2, and C_2H_4 products at the 21st hour of the ESR process at 500°C under various conditions (ethanol-to-water molar ratio of 1 : 4, 1 : 9, and 1 : 12).

disrupted due to strong interactions with water, and the reoxidation process can be more pronounced. The above combined with a higher starting share of Co^{2+} in CoUSY may lead to the dominance of the nonmetallic cobalt fraction in this catalyst and consequently to a reduction of hydrogen and CO_2 formation with a simultaneous increase in the formation of C_2H_4. This stays in good agreement with the report of Inokawa et al. (2010). The rapid C_2H_4 production by ethanol dehydration in the presence of transition Ni^{2+} and Co^{2+} cations in the zeolite Y was ascribed to both the interaction of metal cations with the OH groups of ethanol molecules and the appearance of additional H^+ by the dissociation of water molecules coordinated to cations. Indeed, at high water loading ($EtOH/H_2O$ equal to 1 : 12), nonreduced Co^{2+} cations (see TPR part) withdrawn from sodalite cages and hexagonal prisms can participate in both the binding of ethanol molecules and the hydrolysis process leading to the appearance of an additional number of protons as well. Consequently, the migration of cobalt cation and subsequent hydrolysis process together with reoxidation of metallic cobalt strongly affected the zeolite CoUSY activity. The partial dealumination of the zeolite can be also considered. The formation of extraframework aluminum species can be associated with the insertion of Al^{3+} cations into the Co_3O_4 matrix and progressive formation of the $Co_{3-x}Al_xO_4$ spinel. The ethanol conversion depends on the number of exposed cobalt active sites; thus, the formation of mixed spinel would perturb this number significantly.

CONCLUSIONS

The co-modified USY and ZSM-5 zeolite materials (Si/Al ratio of 31) were synthesized, characterized in terms of the chemical and phase composition, morphology, porosity, reducibility, and acidity, and evaluated in the ESR process at 500°C for various $EtOH/H_2O$ ratios (1 : 4; 1 : 9; and 1 : 12). The undisturbed micropore volume of zeolitic supports followed by a slight enhancement of their mesopore surface areas indicated the effective distribution of the Co_3O_4 phase (10 wt%) in the as-prepared materials. The detailed microscopic studies, together with the quantitative FT-IR studies of Py and CO sorption, confirmed the high dispersion of cobalt species, with the advantage of the CoZSM-5 catalyst with its better availability of cobalt species. Both catalysts showed 100% ethanol conversion, while their selectivity toward products such as H_2, CO_2, C_2H_4, and CH_4 strongly depended on the water content, showing the 1 : 9 ratio as the most effective one. The superior selectivity and stability of the CoZSM-5 catalyst, compared to CoUSY, resulted from enhanced accessibility of cobalt species. In addition, the negative effect of excess water (the $EtOH/H_2O$ molar ratio of 1 : 12) observed for the CoUSY catalyst (significant decrease in selectivity to H_2 and CO_2 and a significant increase to C_2H_4 in comparison for the 1 : 4 ratio) was explained based on the reoxidation of cobalt metallic species.

Since the structure of the zeolite support determines the cobalt active phase dispersion, strongly influencing its performance in the ESR process, it seems interesting to conduct a broader comparison of cobalt catalysts deposited on different zeolite supports in the next step.

DATA AVAILABILITY STATEMENT

The original contributions presented in the study are included in the article/supplementary materials, further inquiries can be directed to the corresponding author/s.

AUTHOR CONTRIBUTIONS

GG and KG were the originators of the concept and planned and supervised the experiments. KP and KT undertook the modification and characterization of materials with the FT-IR of probe molecules studies and assisted in their interpretation. MG planned and carried

out the catalytic testing and assisted in their interpretation. GS carried out the STEM measurements. MR carried out the H_2-TPR testing. GG wrote and edited the final article. All authors have read and agreed to the published version of the article.

FUNDING

This work was financed by Grant No. 2015/18/E/ST4/00191 from the National Science Centre, Poland.

REFERENCES

Ávila-Neto, C. N., Zanchet, D., Hori, C. E., Ribeiro, R. U., and Bueno, J. M. C. (2013). Interplay between particle size, composition, and structure of MgAl2O4-supported Co-Cu catalysts and their influence on carbon accumulation during steam reforming of ethanol. *J. Catal.* 307, 222–237. doi:0.1016/j.jcat.2013.07.025

Alberton, A. L., Souza, M. M. V. M., and Schmal, M. (2007). Carbon formation and its influence on ethanol steam reforming over Ni/Al2O3 catalysts. *Catal. Today.* 123, 257–264. doi:10.1016/j.cattod.2007.01.062

Armor, J. N. (1999). Striving for catalytically green processes in the 21st century. *Appl. Catal. Gen.* 189, 153–162. doi:10.1016/S0926-860X(99)00273-2

Barrett, E. P., Joyner, L. G., and Halenda, P. P. (1951). The determination of pore volume and area distributions in porous substances. I. Computations from nitrogen isotherms. *J. Am. Chem. Soc.* 73, 373–380. doi:10.1021/ja01145a126

Benito, M., Sanz, J. L., Isabel, R., Padilla, R., Arjona, R., and Daza, L. (2005). Bio-ethanol steam reforming: insights on the mechanism for hydrogen production. *J. Power Sources.* 151, 11–17. doi:10.1016/j.jpowsour.2005.02.046

Bineli, A., Tasic, M., and Filho, R. (2016). Catalytic steam reforming of ethanol for hydrogen production: brief status. *Chem. Ind. Chem. Eng. Q.* 22, 327–332. doi:10.2298/CICEQ160216017B

Bion, N., Epron, F., and Duprez, D. (2010). Bioethanol reforming for H2 production. *Catalysis.* 22, 1–55. doi:10.1039/9781847559630-00001

Breen, J. P., Burch, R., and Coleman, H. M. (2002). Metal-catalysed steam reforming of ethanol in the production of hydrogen for fuel cell applications. *Appl. Catal. B Environ.* 39, 65–74. doi:10.1016/S0926-3373(02)00075-9

Calles, J. A., Carrero, A., Vizcaıno, A. J., and Megia, P. J. (2020). Agglomerated Co e Cr/SBA-15 catalysts for hydrogen production through acetic acid steam reforming. *Int. J. Hydrog. Energy.* 45, 15941–15950. doi:10.1016/j.ijhydene.2019.05.237

Campos-Skrobot, F. C., Rizzo-Domingues, R. C. P., Fernandes-Machado, N. R. C., and Cantão, M. P. (2008). Novel zeolite-supported rhodium catalysts for ethanol steam reforming. *J. Power Sources.* 183, 713–716. doi:10.1016/j.jpowsour.2008.05.066

Chen, D., Liu, C., Mao, Y., Wang, W., and Li, T. (2020). Efficient hydrogen production from ethanol steam reforming over layer-controlled graphene-encapsulated Ni catalysts. *J. Clean. Prod.* 252, 119907. doi:10.1016/j.jclepro.2019.119907

Chica, A. (2013). Zeolites: promised materials for the sustainable production of hydrogen. *ISRN Chem. Eng.* 2013, 1–19. doi:10.1155/2013/907425

Chica, A., and Sayas, S. (2009). Effective and stable bioethanol steam reforming catalyst based on Ni and Co supported on all-silica delaminated ITQ-2 zeolite. *Catal. Today.* 146, 37–43. doi:10.1016/j.cattod.2008.12.024

Comas, J., Marino, F., Laborde, M., and Amadeo, N. (2004). Bio-ethanol steam reforming on Ni/Al_2O_3 catalyst. *Chem. Eng. J.* 98, 61–68. doi:10.1016/S1385-8947(03)00186-4

Contreras, J. L., Salmones, J., Colín-Luna, J. A., Nuño, L., Quintana, B., Córdova, I., et al. (2014). Catalysts for H_2 production using the ethanol steam reforming (a review). *Int. J. Hydrog. Energy.* 39, 18835–18853. doi:10.1016/j.ijhydene.2014.08.072

Da Costa-Serra, J. F., and Chica, A. (2011). Bioethanol steam reforming on Co/ITQ-18 catalyst: effect of the crystalline structure of the delaminated zeolite ITQ-18. *Int. J. Hydrog. Energy.* 36, 3862–3869. doi:0.1016/j.ijhydene.2010.12.094

Da Costa-Serra, J. F., Guil-López, R., and Chica, A. (2010). Co/ZnO and Ni/ZnO catalysts for hydrogen production by bioethanol steam reforming. Influence of ZnO support morphology on the catalytic properties of Co and Ni active phases. *Int. J. Hydrog. Energy.* 35, 6709–6716. doi:10.1016/j.ijhydene.2010.04.013

Da Cruz, R. S., Mascarenhas, A. J. S., and Andrade, H. M. C. (1998). Co-ZSM-5 catalysts for N_2O decomposition. *Appl. Catal. B Environ.* 18, 223–231. doi:10.1016/S0926-3373(98)00042-3

Deluga, G. A., Salge, J. R., Schmidt, L. D., and Verykios, X. E. (2004). Renewable hydrogen from ethanol by autothermal reforming. *Science.* 303, 993–997. doi:10.1126/science.1093045

Freni, S. (2001). Rh based catalysts for indirect internal reforming ethanol applications in molten carbonate fuel cells. *J. Power Sources.* 94, 14–19. doi:10.1016/S0378-7753(00)00593-0

Freni, S., Cavallaro, S., Mondello, N., Spadaro, L., and Frusteri, F. (2003). Production of hydrogen for MC fuel cell by steam reforming of ethanol over MgO supported Ni and Co catalysts. *Catal. Commun.* 4, 259–268. doi:10.1016/S1566-7367(03)00051-7

Frusteri, F., Freni, S., Chiodo, V., Donato, S., Bonura, G., and Cavallaro, S. (2006). Steam and auto-thermal reforming of bio-ethanol over MgO and CeO_2 Ni supported catalysts. *Int. J. Hydrog. Energy.* 31, 2193–2199. doi:10.1016/j.ijhydene.2006.02.024

Frusteri, F., Freni, S., Chiodo, V., Spadaro, L., Di Blasi, O., Bonura, G., et al. (2004). Steam reforming of bio-ethanol on alkali-doped Ni/MgO catalysts: hydrogen production for MC fuel cell. *Appl. Catal. Gen.* 270, 1–7. doi:10.1016/j.apcata.2004.03.052

García, E. Y., and Laborde, M. A. (1991). Hydrogen production by the steam reforming of ethanol: thermodynamic analysis. *Int. J. Hydrog. Energy.* 16, 307–312. doi:10.1016/0360-3199(95)00030-H

Góra-Marek, K., Gil, B., and Datka, J. (2009). Quantitative IR studies of the concentration of Co^{2+} and Co^{3+} sites in zeolites CoZSM-5 and CoFER. *Appl. Catal. Gen.* 353, 117–122. doi:10.1016/j.apcata.2008.10.034

Góra-Marek, K., Gil, B., Śliwa, M., and Datka, J. (2007). An IR spectroscopy study of Co sites in zeolites CoZSM-5. *Appl. Catal. Gen.* 330, 33–42. doi:10.1016/j.apcata.2007.06.033

Ghasemzadeh, K., Jalilnejad, E., and Tilebon, S. M. S. (2019). "Chapter 12 - hydrogen production technologies from ethanol,"in *Ethanol: science and engineering.*. Amsterdam, Netherlands: Elsevier. doi:10.1016/B978-0-12-811458-2.00012-2

Gołąbek, K., Tarach, K. A., Filek, U., and Góra-Marek, K. (2018). Ethylene formation by dehydration of ethanol over medium pore zeolites. *Spectrochim. Acta Part A Mol. Biomol. Spectrosc.* 192, 464–472. doi:10.1016/j.saa.2017.11.049

Greluk, M., Rotko, M., and Turczyniak-Surdacka, S. (2020a). Comparison of catalytic performance and coking resistant behaviors of cobalt- and nickel based catalyst with different Co/Ce and Ni/Ce molar ratio under SRE conditions. *Appl. Catal. A Gen.* 590, 117334. doi:10.1016/j.apcata.2019.117334

Greluk, M., Rotko, M., and Turczyniak-Surdacka, S. (2020b). Enhanced catalytic performance of La_2O_3 promoted Co/CeO_2 and Ni/CeO_2 catalysts for effective hydrogen production by ethanol steam reforming. *Renew. Energy.* 155, 378–395. doi:10.1016/j.renene.2020.03.117

Grzybek, G., Ciura, K., Wójcik, S., Gryboś, J., Indyka, P., Inger, M., et al. (2017). On the selection of the best polymorph of Al_2O_3 carriers for supported cobalt nano-spinel catalysts for N_2O abatement: an interplay between preferable surface spreading and damaging active phase-support interaction. *Catal. Sci. Technol.* 7, 5723–5732. doi:10.1039/c7cy01575e

Grzybek, G., Greluk, M., Indyka, P., Góra-Marek, K., Legutko, P., Słowik, G., et al. (2020). Cobalt catalyst for steam reforming of ethanol–Insights into the promotional role of potassium. *Int. J. Hydrog. Energy.* 5, 22658–22673. doi:10.1016/j.ijhydene.2020.06.037

Haga, F., Nakajima, T., Miya, H., and Mishima, S. (1997). Catalytic properties of supported cobalt catalysts or steam reforming of ethanol. *Catal. Lett.* 48, 223–227. doi:10.1023/a:1019039407126

Haryanto, A., Fernando, S., Murali, N., and Adhikari, S. (2005). Current status of hydrogen production techniques by steam reforming of ethanol: a review. *Energy Fuels.* 19, 2098–2106. doi:10.1021/ef0500538

Hou, T., Zhang, S., Chen, Y., Wang, D., and Cai, W. (2015). Hydrogen production from ethanol reforming: catalysts and reaction mechanism. *Renew. Sustain. Energy Rev.* 44, 132–148. doi:10.1016/j.rser.2014.12.023

Hsiao, W. I., Lin, Y. S., Chen, Y. C., and Lee, C. S. (2007). The effect of the morphology of nanocrystalline CeO_2 on ethanol reforming. *Chem. Phys. Lett.* 441, 294–299. doi:10.1016/j.cplett.2007.05.024

Hunter, E. P. L., and Lias, S. G. (1998). Evaluated gas phase basicities and proton affinity of molecules: an update. *J. Phys. Chem. Ref. Data.* 27, 413–656. doi:10.1063/1.556018

Inokawa, H., Nishimoto, S., Kameshima, Y., and Miyake, M. (2010). Difference in the catalytic activity of transition metals and their cations loaded in zeolite for ethanol steam reforming. *Int. J. Hydrog. Energy.* 35, 11719–11724. doi:10.1016/j.ijhydene.2010.08.092

Inokawa, H., Nishimoto, S., Kameshima, Y., and Miyake, M. (2011). Promotion of H_2 production from ethanol steam reforming by zeolite basicity. *Int. J. Hydrog. Energy.* 36, 15195–15202. doi:10.1016/j.ijhydene.2011.08.099

Kaddouri, A., and Mazzocchia, C. (2004). A study of the influence of the synthesis conditions upon the catalytic properties of Co/SiO_2 or Co/Al_2O_3 catalysts used for ethanol steam reforming. *Catal. Commun.* 5, 339–345. doi:10.1016/j.catcom.2004.03.008

Lang, L., Zhao, S., Yin, X., Yang, W., and Wu, C. (2015). Catalytic activities of K-modified zeolite ZSM-5 supported rhodium catalysts in low-temperature steam reforming of bioethanol. *Int. J. Hydrog. Energy.* 40, 9924–9934. doi:10.1016/j.ijhydene.2015.06.016

Łaniecki, M. (2001). "24-P-23-Cu-Y zeolite catalysts for methanol and ethanol steam reforming," In *Studies in surface science and catalysis.*. Editors J. V. A. Galarneau, F. Di Renzo, and F. Fajula (Amsterdam, Netherlands: Elsevier B.V.), 276. doi:10.1016/S0167-2991(01)81605-0

Li, M. R., and Wang, G. C. (2018). The mechanism of ethanol steam reforming on the Co^0 and Co^{2+} sites: a DFT study. *J. Catal.* 365, 391–404. doi:10.1016/j.jcat.2018.07.002

Li, X., Zheng, Z., Wang, S., Sun, C., Dai, R., Wu, X., et al. (2019). Preparation and characterization of core–shell composite zeolite BEA@MFI and their catalytic properties in ESR. *Catal. Lett.* 149, 766–777. doi:10.1007/s10562-018-2638-3

Liguras, D. K., Kondarides, D. I., and Verykios, X. E. (2003). Production of hydrogen for fuel cells by steam reforming of ethanol over supported noble metal catalysts. *Appl. Catal. B Environ.* 43, 345–354. doi:10.1016/S0926-3373(02)00327-2

Llorca, J., Corberán, V. C., Divins, N. J., Fraile, R. O., and Taboada, E. (2013). "Hydrogen from bioethanol," in *Renewable hydrogen technologies.*. Editors L. M. Gandía, G. Arzamendi, and P. M. Diéguez (Amsterdam, Netherlands: Elsevier). doi:10.1016/S0926-3373(02)00327-2

Llorca, J., Homs, N., Sales, J., Fierro, J. L. G., and De La Piscina, P. R. (2004). Effect of sodium addition on the performance of Co-ZnO-based catalysts for hydrogen production from bioethanol. *J. Catal.* 222, 470–480. doi:10.1016/j.jcat.2003.12.008

Llorca, J., Homs, N., Sales, J., and Ramírez de la Piscina, P. (2002). Efficient production of hydrogen over supported cobalt catalysts from ethanol steam reforming. *J. Catal.* 209, 306–317. doi:10.1006/jcat.2002.3643

Maggio, G., Freni, S., and Cavallaro, S. (1998). Light alcohols/methane fuelled molten carbonate fuel cells: a comparative study. *J. Power Sources.* 74, 17–23. doi:10.1016/S0378-7753(98)00003-2

Mattos, L. V., Jacobs, G., Davis, B. H., and Noronha, F. B. (2012). Production of hydrogen from ethanol: review of reaction mechanism and catalyst deactivation. *Chem. Rev.* 112, 4094–4123. doi:10.1021/cr2000114

Mattos, L. V., and Noronha, F. B. (2005). Hydrogen production for fuel cell applications by ethanol partial oxidation on Pt/CeO_2 catalysts: the effect of the reaction conditions and reaction mechanism. *J. Catal.* 233, 453–463. doi:10.1016/j.jcat.2005.04.022

Ni, M., Leung, D. Y. C., and Leung, M. K. H. (2007). A review on reforming bio-ethanol for hydrogen production. *Int. J. Hydrogen Energy.* 32, 3238–3247. doi:10.1016/j.ijhydene.2007.04.038

Ogo, S., and Sekine, Y. (2020). Recent progress in ethanol steam reforming using non-noble transition metal catalysts: a review. *Fuel Process. Technol.* 199, 106238. doi:10.1016/j.fuproc.2019.106238

Ogo, S., Shimizu, T., Nakazawa, Y., Mukawa, K., Mukai, D., and Sekine, Y. (2015). Steam reforming of ethanol over K promoted Co catalyst. *Appl. Catal. Gen.* 495, 30–38. doi:10.1016/j.apcata.2015.01.018

Passos, A. R., Martins, L., Pulcinelli, S. H., Santilli, C. V., and Briois, V. (2014). Effect of the balance between Co(II) and Co(0) oxidation states on the catalytic activity of cobalt catalysts for Ethanol Steam Reforming. *Catal. Today.* 229, 88–94. doi:10.1016/j.cattod.2013.10.080

Passos, A. R., Martins, L., Pulcinelli, S. H., Santilli, C. V., and Briois, V. (2017). Correlation of sol–gel alumina-supported cobalt catalyst processing to cobalt speciation, ethanol steam reforming activity, and stability. *ChemCatChem.* 9, 3918–3929. doi:10.1002/cctc.201700319

Riani, P., Garbarino, G., Cavattoni, T., and Busca, G. (Forthcoming 2020). CO2 hydrogenation and ethanol steam reforming over Co/SiO_2 catalysts: deactivation and selectivity switches. *Catal. Today.*. doi:10.1016/j.cattod.2020.05.002

Rouqerol, J., Llewellyn, P., and Rouqerol, F. (2007). Is the BET equation applicable to microporous adsorbents? *Stud. Surf. Sci. Catal.* 160, 49–56. doi:10.1016/S0167-2991(07)80008-5.

Słowik, G., Greluk, M., and MacHocki, A. (2016). Microscopic characterization of changes in the structure of KCo/CeO_2 catalyst used in the steam reforming of ethanol. *Mater. Chem. Phys.* 173, 219–237. doi:10.1016/j.matchemphys.2016.02.008

Sekine, Y., Nakazawa, Y., Oyama, K., Shimizu, T., and Ogo, S. (2014). Effect of small amount of Fe addition on ethanol steam reforming over Co/Al_2O_3 catalyst. *Appl. Catal. Gen.* 472, 113–122. doi:10.1016/j.apcata.2013.11.026

Sheng, P.-Y., Bowmaker, G. A., and Idriss, H. (2004). The reactions of ethanol over Au/CeO_2. *Appl. Catal. Gen.* 261, 171–181. doi:10.1016/J.APCATA.2003.10.046

Sohn, H., Celik, G., Gunduz, S., Dogu, D., Zhang, S., Shan, J., et al. (2017). Oxygen mobility in pre-reduced nano- and macro-ceria with Co loading: an AP-XPS, in-situ DRIFTS and TPR study. *Catal. Lett.* 147, 2863–2876. doi:10.1007/s10562-017-2176-4

Sohn, H., Soykal, I. I., Zhang, S., Shan, J., Tao, F., Miller, J. T., et al. (2016). Effect of cobalt on reduction characteristics of ceria under ethanol steam reforming conditions: AP-XPS and XANES studies. *J. Phys. Chem. C.* 120, 14631–14642. doi:10.1021/acs.jpcc.6b02490

Song, S., Akande, A. J., Idem, R. O., and Mahinpey, N. (2007). Inter-relationship between preparation methods, nickel loading, characteristics and performance in the reforming of crude ethanol over Ni/Al_2O_3 catalysts: a neural network approach. *Eng. Appl. Artif. Intell.* 20, 261–271. doi:10.1016/j.engappai.2006.06.014

Subramani, V., and Song, C. (2007). Advances in catalysis and processes for hydrogen production from ethanol reforming. *Catalysis.* 20, 65–106. doi:10.1039/b602364a

Tarach, K. A., Tekla, J., Makowski, W., Filek, U., Mlekodaj, K., Girman, V., et al. (2016). Catalytic dehydration of ethanol over hierarchical ZSM-5 zeolites: studies of their acidity and porosity properties. *Catal. Sci. Technol.* 6, 3568–3584. doi:10.1039/c5cy01866h

Torres, J. A., Llorca, J., Casanovas, A., Domínguez, M., Salvadó, J., and Montané, D. (2007). Steam reforming of ethanol at moderate temperature: multifactorial design analysis of Ni/La_2O_3-Al_2O_3, and Fe- and Mn-promoted Co/ZnO catalysts. *J. Power Sources.* 169, 158–166. doi:10.1016/j.jpowsour.2007.01.057

Trimm, D. L. (1999). Catalysts for the control of coking during steam reforming. *Catal. Today.* 49, 3–10. doi:10.1016/S0920-5861(98)00401-5

Vaidya, P. D., and Rodrigues, A. E. (2006). Insight into steam reforming of ethanol to produce hydrogen for fuel cells. *Chem. Eng. J.* 117, 39–49. doi:10.1016/J.CEJ.2005.12.008

Varga, E., Ferencz, Z., Oszkó, A., Erdohelyi, A., and Kiss, J. (2015). Oxidation states of active catalytic centers in ethanol steam reforming reaction on ceria based Rh promoted Co catalysts: an XPS study. *J. Mol. Catal. Chem.* 397, 127–133. doi:10.1016/j.molcata.2014.11.010

Vizcaíno, A. J., Carrero, A., and Calles, J. A. (2007). Hydrogen production by ethanol steam reforming over Cu–Ni supported catalysts. *Int. J. Hydrog. Energy.* 32, 1450–1461. doi:10.1016/J.IJHYDENE.2006.10.024

Wanat, E. C., Venkataraman, K., and Schmidt, L. D. (2004). Steam reforming and water-gas shift of ethanol on Rh and Rh-Ce catalysts in a catalytic wall reactor. *Appl. Catal. Gen.* 276, 155–162. doi:10.1016/j.apcata.2004.08.001

Wang, S., He, B., Tian, R., Wu, X., An, X., and Liu, Y. (2020). Novel core-shell-like Ni-supported hierarchical beta zeolite catalysts on bioethanol steam reforming. *Fuel.* 279, 118449. doi:10.1016/j.ijhydene.2020.04.109

Wang, X., Chen, H. Y., and Sachtler, W. M. H. (2000). Catalytic reduction of NO_x by hydrocarbons over Co/ZSM-5 catalysts prepared with different methods. *Appl. Catal. B Environ.* 26, L227–L239. doi:10.1016/S0926-3373(00)00125-9

Zanchet, D., Santos, J. B. O., Damyanova, S., Gallo, J. M. R., and Bueno, J. M. C. (2015). Toward understanding metal-catalyzed ethanol reforming. *ACS Catal.* 5, 3841–3863. doi:10.1021/cs5020755

Zhang, B., Tang, X., Li, Y., Xu, Y., and Shen, W. (2007). Hydrogen production from steam reforming of ethanol and glycerol over ceria-supported metal catalysts. *Int. J. Hydrog. Energy.* 32, 2367–2373. doi:10.1016/j.ijhydene.2006.11.003

Zhurka, M. D., Lemonidou, A. A., Anderson, J. A., and Kechagiopoulos, P. N. (2018). Kinetic analysis of the steam reforming of ethanol over Ni/SiO_2 for the elucidation of metal-dominated reaction pathways. *React. Chem. Eng.* 3, 883–897. doi:10.1039/c8re00145f

Conflict of Interest: The authors declare that the research was conducted in the absence of any commercial or financial relationships that could be construed as a potential conflict of interest.